ELSEVIER

Nuclear Physics A 690 (2001) 367–381

NUCLEAR PHYSICS A

www.elsevier.nl/locate/npe

Determination of the Gamow–Teller strength function for the neutron-deficient isotopes $^{104–107}$In

M. Karny [a,b,1], L. Batist [c], B.A. Brown [d], D. Cano-Ott [e,1], R. Collatz [f,1], A. Gadea [e,1], R. Grzywacz [a,b], A. Guglielmetti [f,1], M. Hellström [f], Z. Hu [f,1], Z. Janas [a,f], R. Kirchner [f], F. Moroz [c], A. Piechaczek [g,1], A. Płochocki [a], E. Roeckl [f,*], B. Rubio [e], K. Rykaczewski [a,h], M. Shibata [f,1], J. Szerypo [a,1], J.L. Tain [e], V. Wittmann [c], A. Wöhr [g,1]

[a] *Institute of Experimental Physics, University of Warsaw, PL-00681 Warsaw, Poland*
[b] *Department of Physics, University of Tennessee, Knoxville, TN 37996, USA*
[c] *St. Petersburg Nuclear Physics Institute, 188-350 Gatchina, Russia*
[d] *NSCL, Department of Physics and Astronomy, Michigan State University, East Lansing, MI 48824-1321, USA*
[e] *Instituto de Física Corpuscular IFIC, E-46100 Burjassot (Valencia), Spain*
[f] *Gesellschaft für Schwerionenforschung mbH, Planckstr. 1, D-64291 Darmstadt, Germany*
[g] *Instituut voor Kern- en Stralingsfysica, University of Leuven, B-3001 Leuven, Belgium*
[h] *Oak Ridge National Laboratory, PO Box 2008, Oak Ridge, TN 37831, USA*

Received 30 June 2000; revised 23 November 2000; accepted 14 December 2000

Abstract

The Gamow–Teller β decays of the neutron-deficient indium isotopes $^{104–107}$In have been investigated by using total absorption γ-ray spectrometry on mass-separated sources. The experimental Gamow–Teller strength, deduced as a function of the excitation energy in the daughter nuclei $^{104–107}$Cd, is compared to shell-model predictions.

Keywords: RADIOACTIVITY ^{104,105}In [from ^{50}Cr(^{58}Ni, xpyn)] and ^{106,107}In [from ^{52}Cr(^{58}Ni, xpyn)]; Measured E_γ, I_γ; Deduced β-intensity and β-strength distribution; On-line mass separation; Total absorption spectrometer; NaI(Tl) detectors; Ge detectors; Si detectors; NUCLEAR STRUCTURE $^{104–107}$Cd; $^{104–107}$In; Calculated levels; Gamow–Teller strength; SHELL MODEL
PACS: 21.10.-k; 21.60.Cs; 23.40.Hc; 27.60.+j

* Corresponding author.
E-mail address: e.roeckl@gsi.de (E. Roeckl).
[1] For the present address of the coauthor please contact corresponding author.

0375-9474/01/$ – see front matter
PII: S0375-9474(00)00694-1

1. Introduction

One of the particularly interesting features of nuclear structure studies in the region near the doubly magic nucleus ^{100}Sn is the occurrence of fast β transitions related to the Gamow–Teller (GT) transformation of a $\pi g_{9/2}$ proton into a $\nu g_{7/2}$ neutron. A measurable quantity suited for comparison with theoretical predictions is the β strength of this decay mode, defined as:

$$B_{\mathrm{GT}}(E) = \frac{D \cdot I(E)}{f(Q_{\mathrm{EC}} - E) \cdot T_{1/2} \cdot 100}, \tag{1}$$

where $D = 3860(18)$ s is a constant, corresponding to the value of the axial-vector weak-interaction coupling constant g_A for the decay of the free neutron [1,2], I the β intensity normalized to 100% per decay, E the excitation energy in the daughter nucleus, f the statistical rate function, Q_{EC} the total energy released in electron-capture (EC) decay, and $T_{1/2}$ the β-decay half-life. The $B_{\mathrm{GT}}(E)$ distribution, deduced from measurements of $I(E)$, Q_{EC} and $T_{1/2}$, can be compared to the distribution of the squares of the GT-transition matrix elements obtained from model calculations. The quenching of the experimental GT-transition rates with reference to model predictions has been a puzzle for many years. A renormalization of g_A (or of the GT operator) has been applied (see, e.g., [3,4]) in order to account for the missing GT strength in the ^{100}Sn region. This has led to a consistent picture with the GT strength from shell-model calculations being quenched by about a factor of 4–5 compared to experiment [5–7]. However, the underlying β-decay data were not sufficient to conclude on the mass dependence of the hindrance factor in this region of nuclei.

In this paper, we report on an investigation of the β decay of indium isotopes with mass number from 104 to 107. Measurements and data analysis were performed in the same way as for ^{103}In [6]. Therefore we will frequently refer to the latter work as far as details of experimental technique and of the data evaluation are concerned. The main goal of the measurements described here was to determine the $B_{\mathrm{GT}}(E)$ distribution which, according to Eq. (1), can be deduced by measuring $I(E)$, Q_{EC}, and $T_{1/2}$. We performed the measurement of $I(E)$ by using a total absorption spectrometer (TAS), and took the values of Q_{EC} and $T_{1/2}$ from the literature.

In this paper, the principles of the experimental technique and of the data evaluation are described in Sections 2 and 3, respectively. In Section 4 we report on the experimental data obtained with the TAS, while Section 5 is devoted to the discussion of the experimental GT strength in comparison with shell-model calculations. Finally, a summary is given in Section 6.

2. Experimental techniques

2.1. Total absorption spectrometer

The TAS [9] consists of a large NaI crystal (diameter 356 mm, length 356 mm) surrounding the radioactive source, two small silicon (Si) detectors (thickness 450 μm,

diameter 16 mm) above ("top") and below ("bottom") the source, and one germanium (Ge) detector (thickness 10 mm, diameter 16 mm) placed just above the "top" Si detector. The NaI crystal is protected by a combined borax-lead shielding against natural and accelerator-related background. By demanding coincidence with signals from the Si detectors, the β^+-decay component for the nucleus of interest is selected, whereas coincidences with characteristic $K_{\alpha,\beta}$ X rays recorded by the Ge detector can be used to select the EC mode. While a coincidence condition on the appropriate X rays yields unambiguous Z identification, the TAS spectra taken in coincidence with the Si detectors may contain contributions from isobaric contaminants (see, e.g., [6]). The latter effect, which depends upon details of the source preparation (see Section 2.2), has to be taken into account in the data analysis (see, e.g., Section 4.2.2). From the EC and β^+ coincident TAS spectra the *complete* distribution of the β strength can be determined for neutron-deficient isotopes, including low-lying *and* high-lying levels of the respective daughter nuclei.

The total γ-ray efficiency of TAS for mono-energetic photons between 0.2 and 4.0 MeV is above 88%, and its photo-peak efficiency is above 56%. While these high efficiency values as well as their rather weak dependence on the photon energy are promising, the problem of TAS measurements lies in the response function, the shape of which is complex already for single γ-ray sources. Details concerning the simulations of the response function can be found in [6].

2.2. Source preparation

This work deals with the neutron-deficient indium isotopes with mass number A from 104 to 107. We used fusion–evaporation reactions induced by a ^{58}Ni beam on a 3.6 mg/cm^2 thick ^{50}Cr target to produce ^{104,105}In, and on a 3.7 mg/cm thick ^{52}Cr target to produce ^{106,107}In. The energy and intensity of the ^{58}Ni beam on target amounted to 285 MeV and 40–50 particle nA, respectively. The recoiling reaction products were stopped in a graphite catcher inside the gaseous discharge ion source of the GSI on-line separator [10] which provided a 55 keV mass-separated ion beam. The isobaric contaminations of tin and cadmium isotopes were strongly suppressed by choosing a FEBIAD-B2-C ion source with an alternately heated and cooled "cold pocket" which yields "bunched" beams [11] of indium isotopes, temporarily separated from the tin or cadmium isobars. The mass-separated beam, thus chemically purified, was implanted in a transport tape. The resulting source was moved periodically away through a differential pumping system from the collection position (in vacuum) to the center of TAS (in air), where its radioactive decay was measured. The collection (T_{col}) and measurement (T_{meas}) times, used in this work, are listed in Table 1. After three consecutive collection periods, the mass-separated beam was directed for one collection interval to a separate tape collector which was equipped with a standard Ge detector for monitoring intensity and purity of the beam, while simultaneously a background measurement was performed at the TAS. This mode of beam sharing between the TAS and the monitoring station was continued for the total counting times given in Table 1. The choice of T_{col} and T_{meas} was optimized to suppress longer-lived activities such

Table 1
Ground-state properties of the nuclei studied in this work, together with the time parameters of the measurements[a]

Nucleus	I^π	$T_{1/2}$	Q_{EC} (keV) [12]	T_{col} (s)	T_{meas} (s)	T_{tot} (h)
^{104}In	$5, 6(^+)$ [13]	108(2) s [17]	7910(140)	200	200	5
^{105}In	$(9/2)^+$ [14]	5.07(7) min [18]	4849(13)	200	200	9
^{106}In	7^+ [15]	6.2(1) min [19]	6521(11)	200	200	8
^{107}In	$9/2^+$ [16]	32.4(3) min [20]	3426(11)	360	360	3

[a] I denotes the spin, $T_{1/2}$ the half-life, Q_{EC} the total energy available in electron-capture decay, T_{col} and T_{meas} the collection and measurement periods of the data-taking cycle, and T_{tot} the total counting time devoted to the various isotopes studied.

Table 2
Properties of the isomeric states of $^{104–107}$In[a]

Isomer	$T_{1/2}$	E^* (keV)	I^π	b.r.
^{104m}In [13]	15.7(5) s	94	(3^+)	$\beta = 20\%$, $IT = 80\%$
^{105m}In [14]	48(6) s	674	$(1/2^-)$	$IT = 100\%$
^{106m}In [15]	5.2(1) min	29	(2^+)	$\beta = 100\%$
^{107m}In [21]	50.4(6) s	679	$1/2^-$	$IT = 100\%$

[a] E^* denotes the excitation energy of the isomer, I its spin, and b.r. its branching ratio for a specific decay channel. Internal transitions are characterized by IT, and positron decay and electron capture by β.

as the one of the contaminant isobaric silver, which is hardly attenuated by the ion source operation mentioned above.

Decay measurements on $^{104–107}$In are complicated by the existence of long-lived isomers (see Table 2). As the spins of all isomeric states under consideration are lower by a few units than that of the corresponding ground states, it is expected that the heavy-ion reactions used in this work favors the population of the (high-spin) ground states. For isotopes in their ground state, the intensities of the mass-separated beams span from 1.3×10^4 atoms/s for ^{104}In) to 3.5×10^4 atoms/s for ^{107}In, while the corresponding numbers for isomeric states were in the range between 2.5×10^2 for ^{105m}In and 4.8×10^3 for ^{107m}In. While details concerning the contamination by isomers and other isobaric activities will be discussed below, we note already here that the long-lived isomeric states in odd-mass indium isotopes deexcite only via internal transitions, whereas ^{104m}In disintegrates by both internal and β decay, and ^{106m}In only by β decay.

3. General remarks on the data evaluation procedures

In order to deduce the β-intensity $I(E)$ as a function of the excitation energy E in the daughter nucleus from an experimental TAS spectrum $S(x)$, one has to solve the equation

$$S(x) = \sum_i R_i(x) \cdot I_i, \tag{2}$$

where I_i is the β feeding to level i. Any column $R_i(x)$ of the response matrix, transformed from energy into experimental spectrum channels (x), represents the "level response function" of TAS to the cascade of γ rays deexciting the level i. $R_i(x)$ can be calculated recursively by using the response function for the lower levels, as

$$R_i(x) = \sum_{k=0}^{i-1} b_{i\to k} \cdot \int R_k(x') \cdot G(E_i - E_k, x - x')\,\mathrm{d}x', \tag{3}$$

where $G(E, x)$ is the TAS response function to the monoenergetic γ transition of the energy $E = E_i - E_k$, $b_{i\to k}$ the branching ratio for this transition, and $R_k(x)$ the level response function which is reduced to the δ function $\delta(x')$ in the case of a γ transition to the ground state ($k = 0$).

In the case of TAS measurements of exotic nuclei one usually faces the problem that, even though some β-delayed γ rays are known from high-resolution measurements, many of them have escaped from observation in these experiments. Correspondingly, the decay schemes obtained from high-resolution data are incomplete, and hence assumptions have to be made in deducing I_i. For choosing R_i and calculating I, we first introduced, in addition to the states in daughter nucleus known from high-resolution work, "pseudo levels" with an average intralevel spacing of approximately 50 keV. Furthermore, we assumed R_i of a given pseudo level to correspond to the average R_i of all unobserved levels in the vicinity of a pseudo level. Such a procedure appears to be justified because of the poor energy resolution of the NaI. The response function of a pseudo level is constructed in the same way as for the known levels. Once the response functions are established for all levels, we sum them weighted with $I(E)$, and thus construct a simulated spectrum which is then compared with the experimental one. Insufficient assumptions on I and/or R_i result in deviations of the shapes of simulated and experimental spectra. The final solution is found by modifying the primary assumptions and checking the influence of such changes on the results. A more detailed description of this method as well as a discussion on systematic uncertainties can be found in [6].

4. Results and discussion

4.1. Odd-mass indium isotopes

On the basis of the extreme single-particle shell model, two main components are expected [4] in the GT decay of odd-proton nuclei such as indium isotopes, i.e. one related to the transformation of the unpaired $g_{9/2}$ proton, and another one related to the transformation of one of the paired protons from the $\pi g_{9/2}^8$ core, yielding a $[\pi g_{9/2}^{-1} \nu g_{7/2}]_{1^+}$ pair. These components lead to the population of a one-quasiparticle $7/2^+$ and of three-quasiparticle $[[\pi g_{9/2}^{-1} \nu g_{7/2}]_{1^+}(g_{9/2})]_{J^+}$ states, respectively. In all odd-mass indium isotopes investigated in this work we observed a transition to a low-lying

$7/2^+$ state [14,16] in the daughter nucleus, which mainly represents a single-particle excitation of a neutron from $d_{5/2}$ to $g_{7/2}$. Therefore, β-feeding to this level can be associated with the decay of the valence proton. This mode becomes weaker when the Q_{EC} window increases and thus permits transitions to highly excited states in the daughter nucleus, populated in the transformation of a proton from the $(g_{9/2})^8$ core, are possible.

4.1.1. ^{107}In decay

High resolution γ-ray spectroscopy data provided a decay scheme of ^{107}In which comprises 44 levels and 134 γ transitions [16,20]. This scheme was found to be almost sufficient to reproduce the experimental TAS spectrum. Nevertheless, 3 additional pseudo levels had to be added at ^{107}Cd excitation energies of 3.1, 3.2 and 3.3 MeV in order to get agreement between (the high-energy part of) the simulated and experimental spectrum. Examples of the reconstruction of the TAS EC and β^+ spectra are presented in Fig. 1. Neither daughter activity nor other isobaric contaminants were detected in the analyzed TAS spectra.

The total conversion coefficient of the strongest β-delayed γ ray of ^{107g}In, i.e. the 204 keV M1-transition, is much smaller than the corresponding number in the case of ^{105}In, discussed in Section 4.1.2. Thus, the influence of conversion electrons on the analysis of the ^{107}In data can safely be neglected. The insufficient reconstruction of the β^+ spectrum below the 1022 keV peak (see Fig. 1) is due to the simplification made during the calculation of the TAS response function for positrons emitted from the radioactive sample (see [6]).

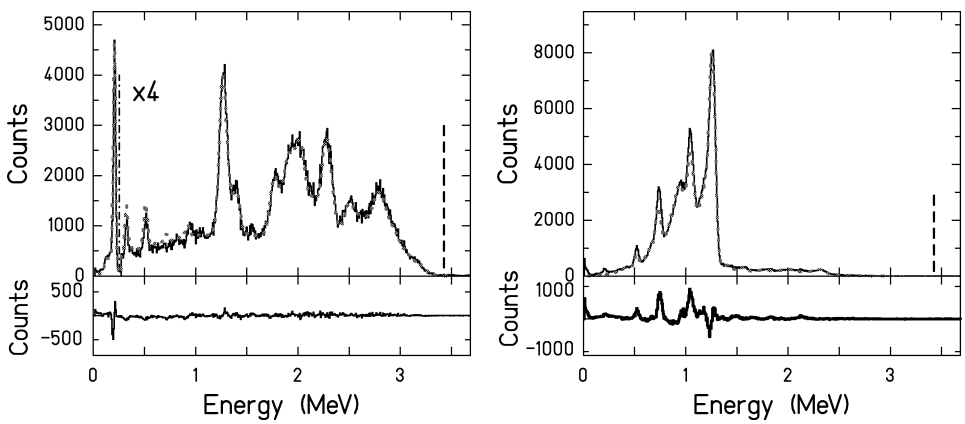

Fig. 1. Upper left panel: experimental (solid line) and simulated (dotted line) TAS spectrum assigned to the EC decay of ^{107}In (note the change of the ordinate scale by a factor of 4 for excitation energies above 250 keV). Lower left panel: difference between experimental and simulated TAS spectra. The right panels show the corresponding experimental, simulated and differential spectra for the positron decay of ^{107}In. The vertical broken lines indicate the Q_{EC} value of 3.426(11) MeV.

4.1.2. ^{105}In decay

In the β-decay measurement of ^{105}In one may expect ^{105}Cd ($T_{1/2} = 55.5(5)$ min [14]) as a main contaminant. As ^{105}Cd was not produced in the reaction, its presence in the TAS spectrum has to be associated with the grow-in as a daughter of ^{105}In. We got rid of the ^{105}Cd contribution by using data collected only during the initial 50 s interval of the 200 s measurement time. The intensity of the ^{105m}In beam, measured by means of the standard Ge detector, amounted to 250 atoms/s, while the corresponding number for ^{105}In is 16400 atoms/s. The internal decay of ^{105m}In (see Table 2) has no influence on the β-decay measurement of ^{105}In.

The initial simulation procedure was based on high-resolution γ-ray data from previous work, which included 34 excited ^{105}Cd levels, 128 γ transitions assigned to the ^{105}Cd level scheme, and 17 γ rays that were assigned to the decay of ^{105}In, but not placed in the decay scheme [14,18]. Subsequently, 27 pseudo-levels were added at ^{105}Cd excitation energies between 2.6 and 4.3 MeV. In Fig. 2 the reconstructions of the β^+ and EC coincident TAS spectra are presented. In the spectrum related to positron decay one can see a significant 1022 keV peak. Although the feeding associated with the 1022 keV peak should indicate a ground state to ground-state transition, in the case of ^{105}In it is interpreted as being due to undetected conversion electrons from the 131 keV transition in ^{105}Cd. This is conceivable as for an M1 transition of this energy the total conversion coefficient α_{tot} is 0.218. Therefore, the apparent feeding to the ^{105}Cd ground state is actually caused by the β^+ feeding to the first excited ^{105}Cd state at 131 keV, followed by the emission of a conversion electron which is stopped in the passive material before reaching the NaI(Tl) crystal.

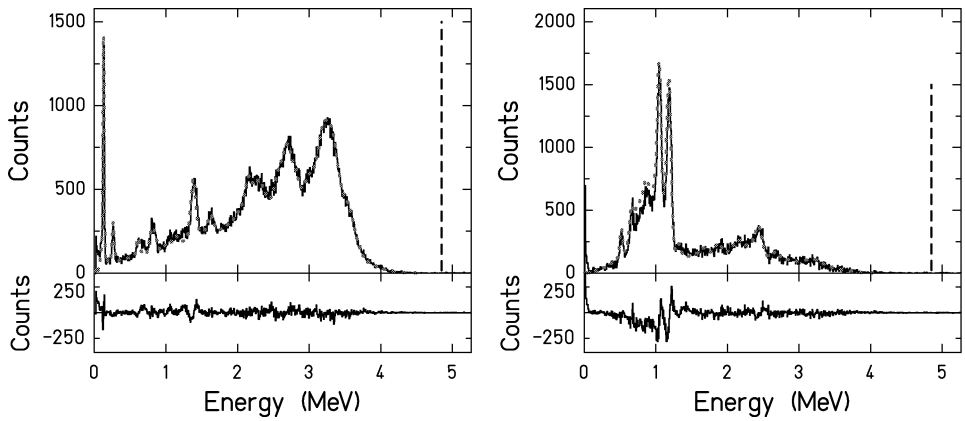

Fig. 2. Upper left panel: experimental (solid line) and simulated (dotted line) TAS spectrum assigned to the EC decay of ^{105}In. Lower left panel: difference between experimental and simulated spectra. The right panels show the corresponding experimental, simulated and differential spectra for the positron decay of ^{105}In. The vertical broken lines indicate the Q_{EC} value of 4.849(13) MeV.

4.2. Even-mass indium isotopes

Within the framework of the extreme single-particle shell model, the β decay of light even-mass indium isotopes is expected to populate two- and four-quasiparticle states in the daughter nucleus with the configurations $[\nu g_{7/2}\nu d_{5/2}]_{J^+}$ and $[[\pi g_{9/2}^{-1}\nu g_{7/2}]_{1^+}\pi g_{9/2}, \nu d_{5/2}]_{J^+}$, respectively.

4.2.1. Decay of ^{106}In and ^{106m}In

^{106}In is produced in the ^{52}Cr(^{58}Ni,3p1n) reaction not only in the ground state but also in the isomeric state. Both states undergo β decay with half-lives of 6.2(1) min [19] and 5.2(1) min [15] for the ^{106}In (7^+) ground state and the ^{106m}In (2^+) isomer, respectively. The very similar half-lives prevented us from decomposing the TAS spectra into separate components related to the decay of ground state and isomer. Therefore, both decay schemes were taken into account for the reconstruction of the experimental spectrum. Such a procedure is justified in view of the large spin difference of the decaying levels, which leads to almost completely separated decay schemes, whose only common features are the two low-lying ^{106}Cd states at 633 and 1494 keV, and the ^{106}Cd levels at 2629 and 2920 keV. All in all, 26 levels including 52 γ transitions, and 24 levels including 38 γ transitions were used in the initial simulation procedure for ^{106}In and ^{106m}In, respectively, with 24 pseudo levels being subsequently added above ^{106}Cd excitation energies of 3.8 MeV. Fig. 3 shows a comparison between the simulated and experimental spectra. Although the feeding associated with the decay of ^{106m}In and ^{106}In to known ^{106}Cd levels can be separated, the feeding to the pseudo levels can not be unambiguously assigned to either of the decays.

The data obtained by using the standard Ge detector showed that the intensity of the ^{106m}In beam amounted to approximately 7.5% relative to that of all $A = 106$ indium atoms implanted on the tape. This translates into a ratio of 8.5% for the corresponding number

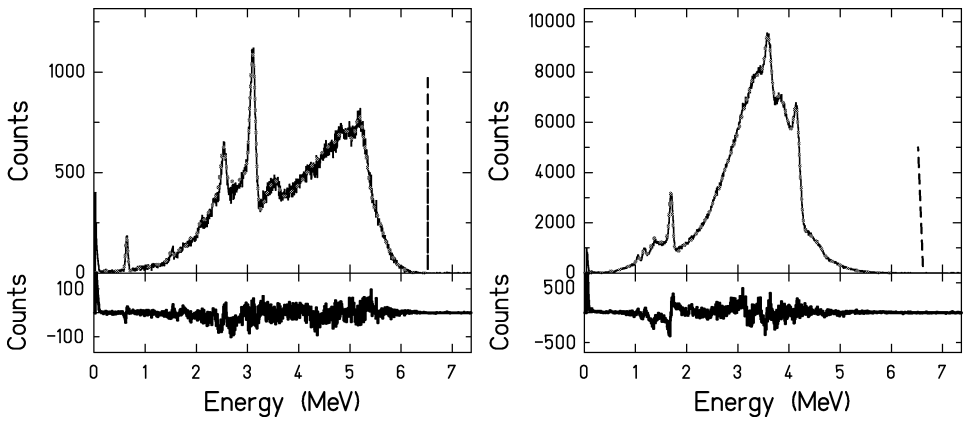

Fig. 3. Upper left panel: experimental (solid line) and simulated (dotted line) TAS spectrum for the EC decay of ^{106}In EC decay. Lower left panel: difference between experimental and simulated spectra. The right panels show the corresponding experimental, simulated and differential spectra for the positron decay of ^{106}In. The vertical broken lines indicate the Q_{EC} value of 6.521(11) MeV.

of decays occurring during the 200 s measurement time (see Table 1). The impact of the ^{106m}In contamination on the B_{GT} value deduced for ^{106}In will be discussed in Section 5.

4.2.2. ^{104}In decay

The β-decay scheme of ^{104}In based on high-resolution studies contains 52 γ transitions and 37 ^{104}Cd levels up to 4.5 MeV excitation energy [22]. Moreover, Ref. [22] lists 72 γ transitions that were not placed in the decay scheme. Our data analysis required the introduction of 32 pseudo-levels in order to approximate the decay pattern to high energies.

Fig. 4 shows the EC and β^+ coincident TAS spectra, obtained for $A = 104$, together with the result of the simulation. The β^+ spectrum shows a distinct peak at a ^{104}Cd excitation energy of about 1600 keV, which can not be reconstructed by using the data known for the ^{104}In decay (see inset in Fig. 4). The time analysis of this peak indicates that it has to be assigned to a longer-lived activity, a possible explanation being the decays of ^{104}Cd and/or ^{104}Ag. ^{104}Cd, however, decays almost completely by electron capture ($Q_{EC} = 1137(11)$ keV [12]), and should therefore not occur in the positron-coincident spectrum. In the case of silver isotopes with $A = 104$, there is a 2^+ isomer known with a half-live of 33.5(20) min [23]. Its decay by positron emission to the first excited 2^+ level at 556 keV in ^{104}Pd is evidently responsible for the 1600 keV peak mentioned above. The 5^+ ground state of ^{104}Ag can not directly populate the 556 keV state, and does therefore not contribute to this peak. Since the positron decay of ^{104m}Ag is characterized by a 93% feeding of the 556 keV level [23], only this state was added in the reconstruction of the $A = 104$ TAS spectrum. The simulated spectrum, which includes the ^{104}In decay together with the ^{104m}Ag β transition to the 556 keV level, is presented in Fig. 4. No contamination by ^{104m}In was traced during this analysis.

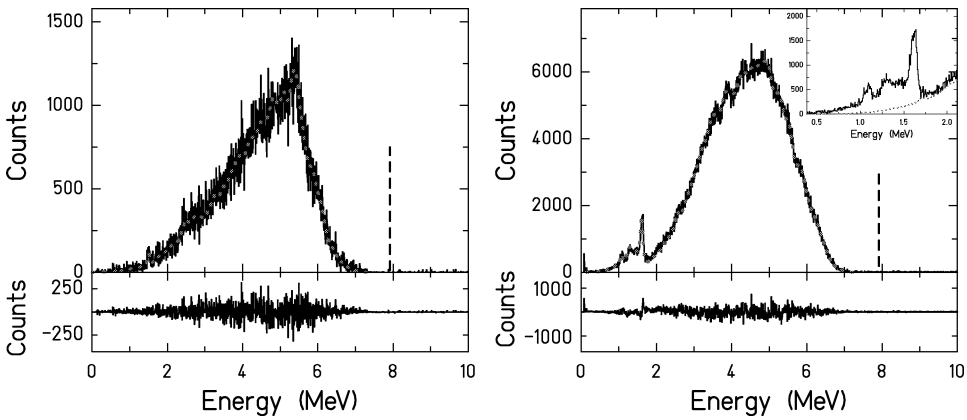

Fig. 4. Upper left panel: experimental (solid line) and simulated (dotted line) TAS spectrum for the EC decay of ^{104}In EC decay. Lower left panel: difference between experimental and simulated spectra. The right panels show the corresponding experimental, simulated and differential spectra for the positron decay of ^{104}In. The vertical broken lines indicate the Q_{EC} value of 7.91(14) MeV. Inset: low-energy part of the experimental $A = 104$ positron spectrum in comparison to the ^{104}In simulation, obtained by neglecting the contamination of ^{104m}Ag.

5. Comparative discussion of the B_{GT} distributions

5.1. Experimental data

The experimentally derived B_{GT} distributions for $^{104-107}$In are presented in Fig. 5, while the summed experimental B_{GT} values ($\sum B_{GT}^{exp}$), obtained by integrating over the entire experimental B_{GT} distribution, are listed in Table 3. In all cases, transitions associated with *core* decay are dominant, although it is evident that for the heavier indium isotopes some strength is also related to the valence-proton decay mode. The *strong* β feeding of low-lying daughter states, e.g. 27% and 33%, observed for the decays of ^{105}In and ^{107}In, respectively, yields only a *small* contribution to $\sum B_{GT}^{exp}$ due to the influence of the statistical rate function (see Eq. (1)).

The experimental B_{GT} data of ^{106}In presented in Fig. 5 include the decay of both ground state and isomeric state, the "combined" $\sum B_{GT}^{exp}$ value amounting to 1.4(3). The shell-model calculation, which will be described in detail below, predicts the B_{GT} distribution of ^{106m}In to be concentrated at ^{106}Cd excitation energies of about 4.5 MeV (see Fig. 6). If this prediction properly described the ^{106m}In decay, the contribution of the latter to the combined $\sum B_{GT}^{exp}$ value for $A = 106$ could be over-estimated under the following assumption:

(i) all (100%) β-decays of ^{106m}In go to the ^{106}Cd level at 4.5 MeV,
(ii) 8.5% of the total number of TAS events for the decay of $A = 106$ indium nuclei is assigned to be related to the ^{106m}In β-decay (see Section 4.2.1),
(iii) identical half-lives are assumed for ^{106}In and ^{106m}In.

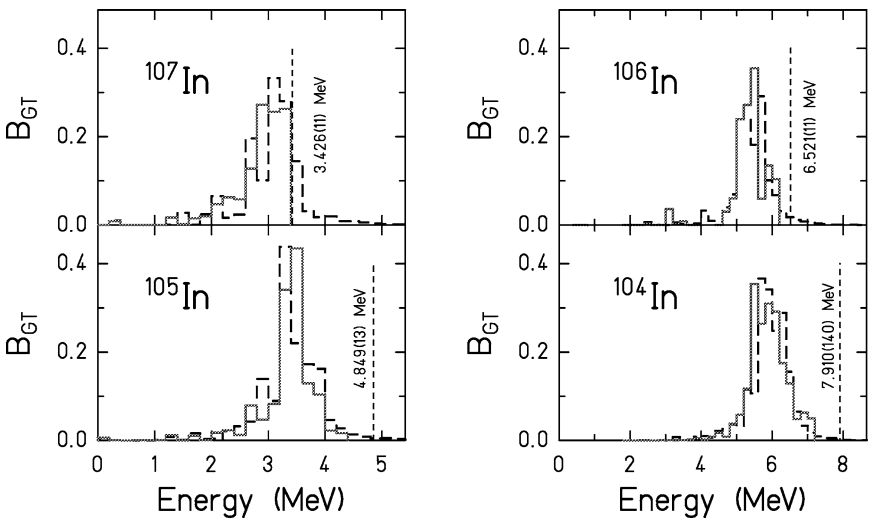

Fig. 5. Gamow–Teller strength distributions for $^{104-107}$In measured with the Total Absorption Spectrometer (solid line) and calculated within the truncated SNC model space (broken line). The relative uncertainties of the experimental results are about 20% except for excitation energies close to the Q_{EC} values (see text). The theoretical Gamow–Teller strength values have been scaled down by the *h* factors from Table 3. The vertical dashed lines indicate the Q_{EC} values.

Table 3
Calculated $\sum B_{GT}^{SNC}$ and $\sum B_{GT}^{SNC'}$ values for $^{99-107}$In in comparison with experimental $\sum B_{GT}^{exp}$ values for $^{104-107}$In (this work) and ^{103}In [6]. In addition, the SNC results for the occupancy factor $N_{7/2}$ of the $\nu g_{7/2}$ orbital are listed as calculated with the assumption of $N_{9/2} = 9.0$. The centroids of the theoretical and experimental B_{GT} distributions ($\overline{E}_{theo}$,$\overline{E}_{exp}$), the cut-off energies E_{cut} used to calculate $\sum B_{GT}^{SNC'}$, and the hindrance factors h are also presented. See text for details

Nucleus	J	$N_{7/2}/8$	$\sum B_{GT}^{SNC}$	$\overline{E}_{theo}$	$\overline{E}_{exp}$	E_{cut}	$\sum B_{GT}^{SNC'}$	$\sum B_{GT}^{exp}$	h
^{99}In	9/2	0	16.0	4.3	–	–	–	–	–
^{100}In	5	0.006	15.9	6.0	–	–	–	–	–
	6	0.013	15.8	6.2	–	–	–	–	–
	7	0.069	14.9	6.3	–	–	–	–	–
^{101}In	9/2	0.149	13.7	4.0	–	–	–	–	–
^{102}In	5	0.169	13.3	5.6	–	–	–	–	–
	7	0.181	13.1	6.1	–	–	–	–	–
^{103}In	9/2	0.250	12.0	3.7	3.70(10)	–	12.0	2.47(25)	4.9(5)
^{104}In	3	0.275	11.6	5.0	–	–	–	–	–
	6	0.306	11.1	5.9	5.90(5)	7.36	11.0	1.9(3)	5.8(9)
^{105}In	9/2	0.356	10.3	3.4	3.34(5)	4.52	10.1	1.4(2)	7.2(10)
^{106}In	2	0.369	10.1	4.7	–	–	–	–	–
	7	0.394	9.7	5.4	5.45(10)	6.43	9.4	1.4(3)	6.7(14)
^{107}In	9/2	0.481	8.3	3.1	–	3.43	6.8	$\geqslant$ 1.1(2)	$\leqslant$ 6.2(1.1)

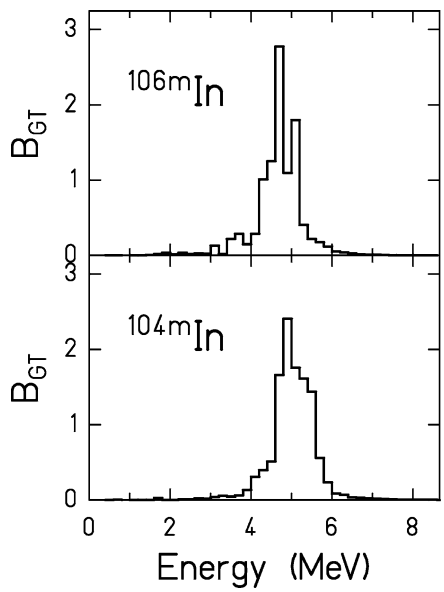

Fig. 6. Theoretical calculation of the B_{GT} distributions in the SNC model space for the decay of low-spin isomeric states in ^{106}In and ^{104}In.

The assumption (i) gives an overestimated value of 1.1 for $\sum B_{\mathrm{GT}}^{\mathrm{exp}}$, which should further be multiplied by 8.5% due to the assumption (ii). Thus, the total ^{106m}In contribution to $\sum B_{\mathrm{GT}}^{\mathrm{exp}}$ for the decay of $A = 106$ indium nuclei would be 0.09, i.e. smaller than the experimental uncertainty of the $\sum B_{\mathrm{GT}}^{\mathrm{exp}}$ value. On the basis of these semiempirical arguments, the $\sum B_{\mathrm{GT}}^{\mathrm{exp}}$ value of 1.4(3) (see Table 3) can be considered to be representative for the ^{106}In decay without much contribution from ^{106m}In.

The uncertainties of the $B_{\mathrm{GT}}^{\mathrm{exp}}$ data were derived from a least-squares analysis of the differences between the experimental and the simulated TAS spectra, displayed in Figs. 1–4. The uncertainties were found to be about 20% up to excitation energies in the daughter nuclei that are 0.5 MeV below the Q_{EC} value. The statistical uncertainties do not exceed 5% for this range of excitation energies, but strongly increase when approaching the Q_{EC} value more closely. As can be seen from Fig. 5, the $B_{\mathrm{GT}}^{\mathrm{exp}}$ distributions apparently do not extend to excitation energies close to the Q_{EC} value, except for ^{107}In. Correspondingly, the accuracy of the $\sum B_{\mathrm{GT}}^{\mathrm{exp}}$ results for $^{103-106}$In in Table 3, is mainly limited by the systematical uncertainties, whereas only an upper limit of $\sum B_{\mathrm{GT}}^{\mathrm{exp}}$ can be given for ^{107}In (see Table 3). The latter restriction is related to the observation that most of the GT strength of ^{107}In is located just below the Q_{EC} value (see Fig. 5). This feature leads to a dramatic increase of the statistical and systematical $B_{\mathrm{GT}}^{\mathrm{exp}}$ uncertainties, the latter contribution being caused by the unknown location of daughter levels near the Q_{EC} value (see also Section 5.2).

5.2. Theoretical calculations

We based the analysis of the strength distribution upon the SNB basis defined in [3]. The *SNB model space* consists of the $1p_{1/2}$, $0g_{9/2}$, $0g_{7/2}$, $1d_{5/2}$, $1d_{3/2}$, $2s_{1/2}$ and $0h_{11/2}$ orbitals. The *SNB basis* consists of a limited set of configurations within the SNB model space in which the active protons are restricted to the $1p_{1/2}$ and $0g_{9/2}$ orbitals, the $1p_{1/2}$ and $0g_{9/2}$ orbitals for neutrons are always filled, and the active neutrons are restricted to the $0g_{7/2}$, $1d_{5/2}$, $1d_{3/2}$, $2s_{1/2}$ and $0h_{11/2}$ orbitals. ^{100}Sn is a closed-shell nucleus in the SNB basis. Thus, GT results obtained in the calculation should be interpreted in this context. In particular, there are ground-state correlations in ^{100}Sn which have the effect of reducing the total GT strength by factors of 2–3 [4,7,8], but we have suggested in [3,7] that the ground-state correlations do not significantly change the shape of the GT strength distribution from that obtained in the SNB basis. Such correlations exist in all nuclei around ^{100}Sn, and their effect on the total GT strength may be N and Z dependent [4,7,8]. Comparisons for the absolute GT strength which take into account these correlations for the $N = 50$ nuclei have been made previously [7]. For the heavier indium isotopes the effect of ground-state correlations outside the SNB basis is more difficult to evaluate, and the interpretation of the total GT strengths will be left to a future work. In this paper we discuss the distribution of the GT strength and the total B_{GT} value within the SNB model space in comparison to experimental data.

The calculations were carried out with the SNC interaction of [7]. The SNC interaction is a modification of the SNB interaction used in [3] in which the normalization of the proton–

neutron G matrix was increased from $N_{pn} = 0.70$ (SNB) to $N_{pn} = 0.77$ (SNC) in order to reproduce the centroid of the GT resonance observed in β decay of ^{97}Ag [7]. Because of limited computer power the calculations were actually performed in the "small" model space described in [6] with the active orbitals $\pi p_{1/2}$ and $\pi g_{9/2}$ for protons and $\nu g_{7/2}$ and $\nu d_{5/2}$ for neutrons. For the lighter indium isotopes where the SNB model space can be used, we have checked that the "small" model space gives essentially the same results for the GT strength distribution as the SNB model space (in which the $1d_{3/2}$, $2s_{1/2}$ and $0h_{11/2}$ neutron orbitals are also included).

Figs. 5 and 6 show the theoretical B_{GT} distributions for ground state and isomeric β-decays of the neutron-deficient indium $^{104–107}$In. The results for the total strength $\sum B_{\mathrm{GT}}^{\mathrm{SNC}}$ and the centroid $\overline{E}$ of the GT distributions are given in Table 3 for a large range of indium isotopes. In these calculations the total strength can be related to the occupation numbers of the initial ground state:

$$\sum B_{\mathrm{GT}}^{\mathrm{SNC}} = \frac{N_{9/2}}{10} \cdot \left(1 - \frac{N_{7/2}}{8}\right) \cdot B_{\mathrm{GT}}^{0}, \tag{4}$$

where $N_{9/2}$ denotes the number of protons filling the $g_{9/2}$ orbit, $N_{7/2}$ the corresponding value for the neutrons on the $g_{7/2}$ orbit, and $B_{\mathrm{GT}}^{0} = 17.78$ the calculated $\sum B_{\mathrm{GT}}$ value of ^{100}Sn. Assuming $N_{9/2} = 9$, one can calculate the occupancy factors $N_{7/2}$ for the $g_{7/2}$ neutron orbit, which are presented in Table 3. The slow reduction of $\sum B_{\mathrm{GT}}^{\mathrm{SNC}}$ with increasing mass number reflects the filling of $g_{7/2}$ neutron orbit. For the odd–odd indium isotopes, there are several nearly degenerate levels at low excitation energy, and we give in Table 3 the results for several possibilities which are suggested by experiment and theory.

Excellent agreement has been achieved between theory and experiment with respect to both shapes and centroids of the B_{GT} distributions (see Fig. 5 and Table 3). Nevertheless, hindrance factors h have to be implied in order to get a quantitative agreement between theory and experiment. For each case h is defined as

$$h = \frac{\sum B_{\mathrm{GT}}^{\mathrm{SNC}'}}{\sum B_{\mathrm{GT}}^{\mathrm{exp}}}, \tag{5}$$

where $\sum B_{\mathrm{GT}}^{\mathrm{SNC}'}$, in contrast to $\sum B_{\mathrm{GT}}^{\mathrm{SNC}}$, was obtained by summing the calculated B_{GT} values from excitation energy 0 in the daughter nucleus to a cut-off energy (E_{cut}). The latter was defined as the lower of the following two quantities, i.e. the Q_{EC} value (i.e. ^{107}In) or the excitation energy that is larger by the TAS energy resolution (FWHM) than the highest lying pseudo level used to reconstruct the experimental TAS spectrum (i.e. $^{104-106}$In). The values of $\sum B_{\mathrm{GT}}^{\mathrm{SNC}'}$ and E_{cut} are also included in Table 3.

As can be seen from Table 3, $\sum B_{\mathrm{GT}}^{\mathrm{exp}}$ decreases from 2.47(25) to 1.1(2) when going from ^{103}In to ^{107}In. While this trend is established at a level of 3.6σ, the present experimental uncertainties are too large to evidence the corresponding trend of the h values. An increase of h with increasing number of $\nu g_{7/2}$ neutrons could be ascribed either to the increasing role of the truncation of the SNC model space or to the increasing limitation of the B_{GT} measurement. The latter argument undoubtedly holds for the case of ^{107}In. Here, systematical and statistical uncertainties in the determination of β intensities for ^{107}Cd

excitation energies close to the Q_{EC} value make it very difficult to reliably deduce $\sum B_{GT}^{exp}$ and h. For example, almost 40% of $\sum B_{GT}^{exp}$ is associated with a β intensity of only 2.8%. Therefore, we restrict ourselves to giving for ^{107}In only a lower limit for $\sum B_{GT}^{exp}$ and an upper limit for h (see Table 3).

6. Summary

We have used the Total Absorption Spectrometer at the GSI on-line separator to measure the β-intensity distribution for neutron-deficient isotopes near ^{100}Sn, i.e. $^{104–107}$In, and to extract information on Gamow–Teller strength function for these decays. Excellent agreement in shape and centroid has been obtained between the experimental strength distributions and SNC shell-model predictions, if the latter are reduced by a hindrance factor. This agreement strongly supports the interpretation that most of the strength is due to the Gamow–Teller transformation of a proton from the $(\pi g_{9/2})^8$ core to a $\nu g_{7/2}$ neutron.

In this work, we obtained for the first time data on the mass dependence of the summed experimental Gamow–Teller strength and on the Gamow–Teller hindrance factor of light indium isotopes. While the former quantity tends to decrease when going from ^{103}In to ^{106}In, the present accuracy of the experimental data does not allow us to draw definite conclusions on a corresponding increase of the latter parameter. In order to remedy this ambiguity it would be interesting to improve the accuracy of Gamow–Teller strength measurements for the isotopes investigated in this work and to extend them to even lighter indium isotopes, where the limitation due to truncation of the shell-model space is less stringent. Experiments of the latter kind are in preparation.

Acknowledgements

This work was supported in part by the Polish Committee of Scientific Research under Grant No. KBN 2 P03B 086 17, by the Program for Scientific Technical Collaboration (WTZ) under Project No. POL 99/009 and RUS 98/672, by the CICYT (Spain) under contract number AEN96-1662 and by the US National Science Foundation under Grant No. 9605207, and by the European Community under Contract No. ERBFMGECT950083. Nuclear physics research at The University of Tennessee is supported by the US Department of Energy through Contract No. DE-FG02-96ER40983. ORNL is managed by UT-Battelle, LLC, for the US Department of Energy under Contract DE-AC05-00OR22725.

References

[1] E. Klempt, P. Bob, L. Hornig, J. Last, S.J. Freedman, D. Dubbers, O. Schärpf, Z. Phys. C 37 (1988) 179.
[2] S.J. Freedman, Comments Nucl. Part. Phys. 19 (1990) 209.
[3] B.A. Brown, K. Rykaczewski, Phys. Rev. C 50 (1994) R2270.

[4] I.S. Towner, Nucl. Phys. A 444 (1985) 402.
[5] A. Płochocki, K. Rykaczewski, T. Batsch, J. Szerypo, J. Żylicz, R. Barden, O. Klepper, E. Roeckl, D. Schardt, H. Gabelmann, P. Hill, H. Ravn, T. Thorsteinsen, I.S. Grant, H. Grawe, P. Manakos, L.D. Skouras, ISOLDE collaboration, Z. Phys. A 342 (1992) 43.
[6] M. Karny, L. Batist, B.A. Brown, D. Cano-Ott, R. Collatz, A. Gadea, R. Grzywacz, A. Gulgielmetti, M. Hellström, Z. Hu, Z. Janas, R. Kirchner, F. Moroz, A. Piechaczek, A. Płochocki, E. Roeckl, B. Rubio, K. Rykaczewski, M. Shibata, J. Szerypo, J.L. Tain, V. Wittmann, A. Wöhr, Nucl. Phys. A 640 (1998) 3.
[7] Z. Hu, L. Batist, J. Agramunt, A. Algora, B.A. Brown, D. Cano-Ott, R. Collatz, A. Gadea, M. Gierlik, M. Górska, H. Grawe, M. Hellström, Z. Janas, M. Karny, R. Kirchner, F. Moroz, A. Płochocki, M. Rejmund, E. Roeckl, B. Rubio, M. Shibata, J. Szerypo, J.L. Tain, V. Wittmann, Phys. Rev. C 60 (1999) 024315.
[8] S.E. Koonin, D.J. Dean, K. Langanke, Phys. Rep. 278 (1997) 1;
D.J. Dean, S.E. Koonin, T.T.S. Kuo, K. Langanke, P.D. Radha, Phys. Lett. B 367 (1996) 17.
[9] M. Karny, J.M. Nitschke, L.F. Archambault, K. Burkard, D. Cano-Ott, M. Hellström, W. Hüller, R. Kirchner, S. Lewandowski, E. Roeckl, A. Sulik, Nucl. Instrum. Methods Phys. Res. B 126 (1997) 320.
[10] K. Burkard, R. Collatz, M. Hellström, Z. Hu, W. Hüller, O. Klepper, R. Kirchner, E. Roeckl, K. Schmidt, M. Shibata, A. Weber, Nucl. Instrum. Methods Phys. Res. B 126 (1997) 12.
[11] R. Kirchner, Nucl. Instrum. Methods Phys. Res. B 26 (1987) 204.
[12] G. Audi, A.H. Wapstra, Nucl. Phys. A 565 (1993) 1.
[13] J. Blachot, Nucl. Data Sheets 64 (1991) 1.
[14] D. De Frenne, E. Jacobs, Nucl. Data Sheets 68 (1993) 935.
[15] D. De Frenne, E. Jacobs, Nucl. Data Sheets 72 (1994) 1.
[16] J. Blachot, Nucl. Data Sheets 62 (1991) 709.
[17] J. Szerypo, M. Huyse, G. Reusen, P. Van Duppen, Z. Janas, H. Keller, R. Kirchner, O. Klepper, A. Piechaczek, E. Roeckl, D. Schardt, K. Schmidt, R. Grzywacz, M. Pfützner, A. Płochocki, K. Rykaczewski, J. Żylicz, G.D. Alkhazov, L. Batist, A. Bykov, V. Wittmann, B.A. Brown, Nucl. Phys. A 584 (1995) 221.
[18] J. Verplancke, E. Coenen, K. Cornelis, M. Huyse, G. Lhersonneau, P. Van Duppen, Z. Phys. A 315 (1984) 307.
[19] H. Huang, B.P. Pathak, J.K.P. Lee, Can. J. Phys. 56 (1978) 936.
[20] B. Nyman, A. Johansson, W. Dietrich, A. Bäcklin, H. Pattersson, B. Svahn, C.O. Lannergad, Phys. Scr. 7 (1973) 265.
[21] H.-C. Hseuh, E.S. Macias, Phys. Rev. C 14 (1976) 345.
[22] J. Vanhorenbeeck, E. Coenen, P. Decrock, P. Dendooven, K. Deneffe, M. Huyse, G. Reusen, P. van Duppen, J. Wauters, P. del Marmol, Phys. Rev. C 39 (1989) 1528.
[23] J. Blachot, J.P. Husson, J. Oms, G. Berrier, Nucl. Data Sheets 41 (1984) 325.